

Article

Effect of Ion Energy on the Microstructure and Properties of Titanium Nitride Thin Films Deposited by High Power Pulsed Magnetron Sputtering

Donglin Ma ¹, Qiaoyuan Deng ^{2,3}, Huaiyuan Liu ² and Yongxiang Leng ^{2,*}

¹ College of Physics and Engineering, Chengdu Normal University, Chengdu 611130, China; mdl208115@163.com

² Key Laboratory of Advanced Technologies of Materials, Ministry of Education, School of Materials Science and Engineering, Southwest Jiaotong University, Chengdu 610031, China; dengqiaoyuan2013@163.com (Q.D.); txwhliu@163.com (H.L.)

³ School of Materials Science and Engineering, Hainan University, Haikou 570228, China

* Correspondence: yxleng@home.swjtu.edu.cn

Abstract: Titanium nitride (Ti-N) thin films are electrically and thermally conductive and have high hardness and corrosion resistance. Dense and defect-free Ti-N thin films have been widely used in the surface modification of cutting tools, wear resistance components, medical implantation devices, and microelectronics. In this study, Ti-N thin films were deposited by high power pulsed magnetron sputtering (HPPMS) and their plasma characteristics were analyzed. The ion energy of Ti species was varied by adjusting the substrate bias voltage, and its effect on the microstructure, residual stress, and adhesion of the thin films were studied. The results show that after the introduction of nitrogen gas, a Ti-N compound layer was formed on the surface of the Ti target, which resulted in an increase in the Ti target discharge peak power. In addition, the total flux of the Ti species decreased, and the ratio of the Ti ions increased. The Ti-N thin film deposited by HPPMS was dense and defect-free. When the energy of the Ti ions was increased, the grain size and surface roughness of the Ti-N film decreased, the residual stress increased, and the adhesion strength of the Ti-N thin film decreased.

Keywords: high power pulsed magnetron sputtering; Ti-N; ion energy; microstructure; residual stress; adhesion strength



Citation: Ma, D.; Deng, Q.; Liu, H.; Leng, Y. Effect of Ion Energy on the Microstructure and Properties of Titanium Nitride Thin Films Deposited by High Power Pulsed Magnetron Sputtering. *Coatings* **2021**, *11*, 579. <https://doi.org/10.3390/coatings11050579>

Academic Editor: Alessio Lamperti

Received: 13 April 2021

Accepted: 11 May 2021

Published: 17 May 2021

Publisher's Note: MDPI stays neutral with regard to jurisdictional claims in published maps and institutional affiliations.



Copyright: © 2021 by the authors. Licensee MDPI, Basel, Switzerland. This article is an open access article distributed under the terms and conditions of the Creative Commons Attribution (CC BY) license (<https://creativecommons.org/licenses/by/4.0/>).

1. Introduction

Titanium nitride (Ti-N) thin films are widely used in the surface modification of cutting tools, wear resistance components, and medical implantation devices owing to their advantages of high hardness, electrical and thermal conductivity, and corrosion resistance [1]. Direct current magnetron sputtering (DCMS) techniques have been widely used for the deposition of Ti-N thin films. However, DCMS is characterized by a low ion fraction of the sputtered species, which results in loose structures and defects, such as holes and cracks in thin films, and limits its application in the surface modification of wear- and corrosion-resistant components [2]. Recently, high power pulsed magnetron sputtering (HPPMS) has been employed to deposit dense and defect-free Ti-N thin films [3] or as an additional tool to manipulate the ionization degree in the plasma during Ti-N thin films deposited by DCMS [4]. It offers high power density at a low duty cycle [5] resulting in unique plasma characteristics, such as high sputtering species ionization degree and ion energy [6], which are beneficial for the deposition of dense and defect-free TiN thin films for the surface modification of wear- and corrosion-resistant components [7]. For example, a study by Elmkhah et al. demonstrated that the Ti-N thin film deposited by HPPMS had a dense and defect-free structure and better corrosion resistance than that of the thin film deposited by DCMS [8]. HPPMS deposited Ti-N thin film can protect activated metals such as depleted uranium from aerated neutral NaCl solution corrosion [9]. In addition, the

drawbacks of low deposition rate of HPPMS can be alleviated by using low magnetic field strength [10], introduction of MF pulses during off-time of HPPMS [11], and regulating the pulse-on time and frequency into an optimum value [12].

During the deposition of Ti-N thin film by HPPMS, a substrate bias applied to the substrate further increases the energy of the Ti and N ions, which is beneficial for dense and defect-free Ti-N thin film deposition [13]. However, the high-energy ion bombardment increases the residual stress of the thin films [14], which results in the peeling-off of thin films and thus, catastrophic failure [15]. In addition, during the Ti-N thin film deposition by HPPMS, a compound layer is formed on the target surface (also known as target poisoning) [13], which affects the discharge and plasma characteristics of the Ti target.

Therefore, in this study, the effect of Ti target poisoning on the target discharge and plasma characteristics, such as plasma flux and plasma composition, was analyzed. In addition, the ion energy was varied by applying different substrate bias voltages, and the effect of the Ti ion energy on the microstructure, residual stress, and adhesion of the Ti-N thin film deposited by HPPMS was studied.

2. Experimental

The Ti-N thin films were deposited by an unbalanced magnetron sputtering system [16]. The substrate is silicon wafer (Si) which were used for thickness, residual stress and microstructure investigation, and stainless steel (316 L, SS) which were used for adhesion test of Ti-N thin films. The distance between the target and the substrate was 60 mm. The base pressure of the deposition chamber was less than 8×10^{-4} Pa. Argon and nitrogen were used as working gas; the flow ratio of argon was 60 sccm and that of nitrogen was 4 sccm. The power system was a HPPMS source (HPS-450D, Chengdu Pulsetech Electrical Co., Ltd., Chengdu, China), which sputtered the Ti target with a pulsed trigger voltage of -800 V, frequency of 200 Hz, and pulse of 150 μ s. Before the deposition of the Ti-N thin film, the Ti target was cleaned by DCMS (2 A) for 5 min and pre-sputtered by argon discharge for 15 min at a pressure of 3.0 Pa and substrate bias of -1500 V. The energy of the Ti and N ions was varied by setting the substrate bias voltage from floating to -150 V by a direct-current bias power supply. To improve the adhesion of the Ti-N thin films, a 200-nm Ti interlayer, deposited by DCMS (2 A, 250 V), was introduced.

For the target discharge analysis, an oscilloscope (TDS-220, Tektronix, Shanghai, China) was used to record the target voltage and current. To study the plasma characteristics, optical emission spectroscopy (OES; AvaSpec-2048-7-USB2, Avantes, Apeldoorn, The Netherlands) was performed [17]. The thickness and surface profiles of the Ti-N thin films were measured using a stylus profiler (XP-2, Ambios, Milpitas, CA, USA) and the residual stress of the thin films was calculated using the wafer curvature method [18]. The crystalline structures of the thin films were analyzed using X-ray diffraction (XRD, X'pert, PANalytical, Almelo, The Netherlands) with Cu-K α radiation generated at 40 kV and 30 mA from a Cu target. The microstructures of the thin films were observed using field-emission scanning electron microscopy (SEM, JSM-7100F, JEOL, Tokyo, Japan) and transmission electron microscopy (TEM, Talos F200X, FEI, Waltham, MA, USA). The surface roughness of the thin films was measured by atomic force microscopy (AFM, Multimode 8, Bruker, Billerica, MA, USA) in tapping mode. The adhesion of the thin films was determined using a scratch tester (MFT-2000, Lanzhou Institute of Chemical Physics, Lanzhou, China) fitted with an Al₂O₃ indenter.

3. Results and Discussion

3.1. Target Discharge and Plasma Characteristics

Figure 1 shows the waveforms of the target voltage and the current of the Ti target sputtering with and without the introduction of nitrogen gas. The target voltage showed a trigger voltage of 800 V at the start at 10 μ s, which was followed by a decrease toward a steady state voltage (V_{ss}) of approximately 350 V regardless of the introduction of nitrogen gas. The target discharge current increased continuously after a delay of 10 μ s, which

could be attributed to the plasma buildup [19], then reached a steady state of 140 A. The peak power of the target discharge was 49.0 kW. After the introduction of nitrogen gas, the stable discharge current of Ti target was 150 A, which was higher than the condition for sputtering without nitrogen gas, and the peak power of target discharge was 52.5 kW.

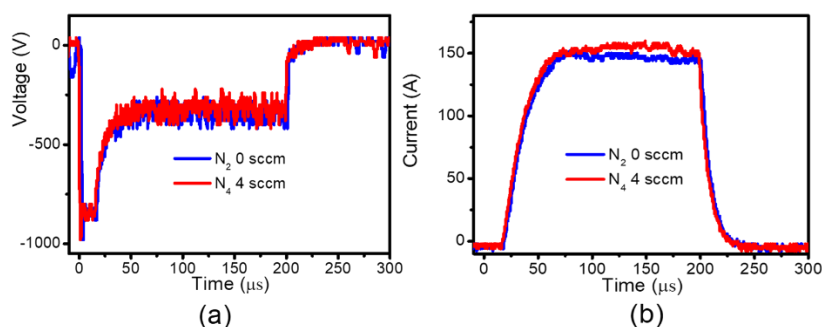


Figure 1. Waveforms of Ti target discharge voltage (a) and current (b) after the introduction of nitrogen gas.

This change in the target discharge current was due to target poisoning. When the nitrogen gas was introduced, the N atoms and ions were adsorbed onto the Ti target surface and formed a nanoscale Ti-N compound layer on it [20]. The secondary electron emission coefficient of the Ti-N compound is higher than that of pure Ti [21], resulting in an increase in the secondary electron current [22], which increases the Ti target discharge current, and thereby the peak power of the target discharge.

Figure 2 shows the OES results of the plasma selected for the analysis of the plasma characteristic such as ions flux and ionized ratio of Ti species with and without the introduction of nitrogen gas. The emission lines mostly consist of Ti^+ (300–380 nm) and Ti^0 (490–525 nm), Ar^+ (450–480 nm), and Ar^0 (650–1000 nm), while the emission lines of N^0 and N^+ were not recorded because of their low intensity. The comparison of Figure 2a,b indicates that after the introduction of the nitrogen gas, the Ti^+ and Ti^0 emission line intensities decreased, because the intensity of the corresponding emission line of the species positively correlated with the plasma flux of the species. Therefore, the decrease in the Ti^+ and Ti^0 emission line intensities can be attributed to a decrease in the plasma flux of the Ti species. After nitrogen gas was introduced, the Ti-N compound layer was formed on the surface of the Ti target. The sputtering yield of Ti-N was lower than that of Ti, resulting in a decrease of the plasma flux of the Ti species sputtered from the target.

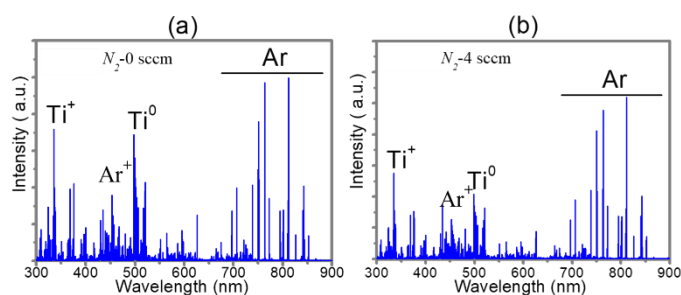


Figure 2. Optical emission spectroscopy of Ti and Ar before (a) and after (b) the introduction of nitrogen gas.

The intensity ratio of Ti^+/Ti^0 was calculated for the ionized ratio of the Ti species. The Ti^+ value is a plus of intensity of emission lines located at 334.90, 334.94, and 336.12 nm and a plus of emission line intensities located at 466.2, 490, and 525 nm representing Ti^0 . The Ti^+/Ti^0 ratio was 1.02 during the sputtering of the Ti target without introducing nitrogen gas, while the Ti^+/Ti^0 ratio was 1.26 when nitrogen gas was introduced. The

OES line intensity is proportional to the concentration of the related species [23]. Thus, these results indicate that after the introduction of nitrogen gas, the ionized ratio of the Ti species increases. After the introduction of nitrogen gas, the Ti-N compound layer was formed on the surface of the Ti target, which increased the Ti target discharge current, and thereby the peak power of the target discharge. The increase in the peak power increases the electron temperature, which promotes the ionization of Ti [24,25]. It should be noted that the ionized ratio of the Ti species is six times than that of DCMS methods [26]; thus, it has the potential for the deposition of more dense and defect-free Ti-N thin films.

3.2. Microstructure and Properties of the Ti-N Thin Film

Figure 3 shows the θ - 2θ XRD results for the Ti-N thin films deposited at different substrate bias values. The crystal structure of the Ti-N thin films deposited on Si was face-centered cubic NaCl type, and the Ti-N (111) diffraction peak was detected in the 2θ range of 36° – 37° . The Ti-N (111) diffraction peak shifted to a lower angle, which was due to the compressive residual stress in the Ti-N thin films, and the shift of the (111) diffraction peak of the Ti-N thin film deposited at a substrate bias of -150 V was larger than that at floating. In addition, the Ti-N thin films exhibited a (111) out-of-plane texture.

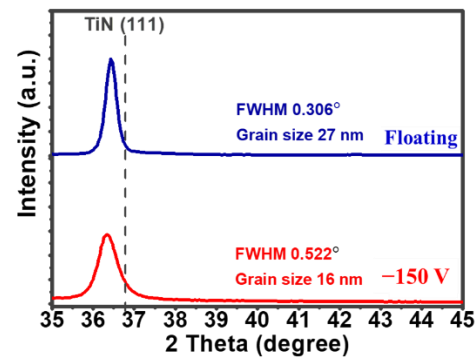


Figure 3. θ - 2θ X-ray diffraction results of the TiN thin films deposited at floating and a substrate bias of -150 V.

During the thin film growth, the competition between the surface diffusion and ion bombardment determines the formation of the crystal texture [27]. A growth condition dominated by surface diffusion tends to form a crystalline texture with the lowest surface energy planes [28], while the growth condition dominated by ion bombardment tends to form crystalline texture with the lowest strain energy planes [29]. In face-centered cubic Ti-N crystals, the (200) plane has the lowest surface energy and the (111) plane has the lowest strain energy [30]. In this study, the Ti-N thin films were deposited by HPPMS, which resulted in a high fraction of ionized Ti, and the Ti ion bombardment provided a Ti-N thin film with crystalline planes with the lowest strain energy, that is, a (111)-textured Ti-N thin film.

The grain sizes of the deposited Ti-N thin films, calculated using the Scherrer formula, were 16 nm at a substrate bias of -150 and 27 nm at floating. During film deposition, the damage due to the high-energy ion bombarding inhibits the grain growth. A higher substrate bias voltage results in a higher ion energy; thus, the grain growth inhibition effect is more noticeable. Therefore, the deposition of the Ti-N thin film at a substrate bias of -150 V resulted in a smaller grain size.

Figure 4 shows high-resolution transmission electron microscopy (HRTEM) images of the Ti-N thin films deposited on Si and SS at floating and a substrate bias of -150 V. It can be seen that the grain size of the deposited Ti-N thin films is ~ 30 nm at floating and ~ 20 nm at a substrate bias of -150 V. These results are in good agreement with the results calculated using the Scherrer formula from the XRD data.

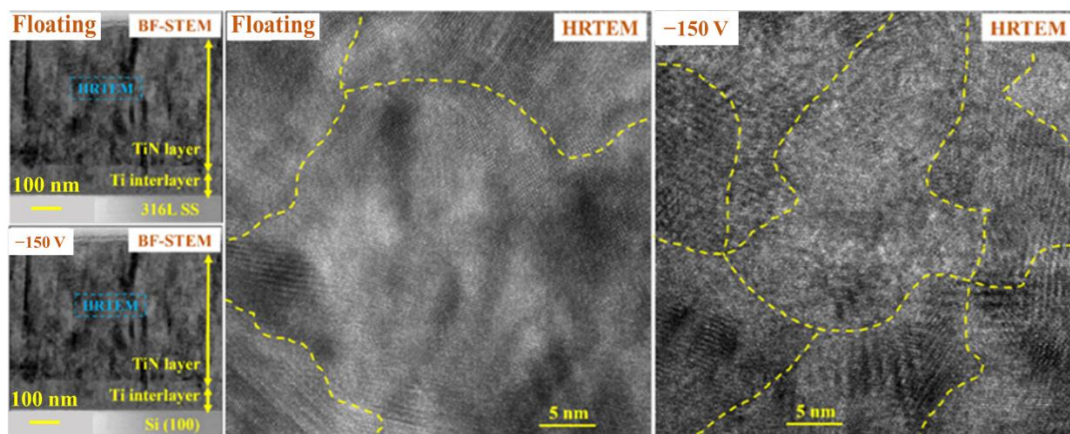


Figure 4. HRTEM morphology of the TiN thin films deposited at floating and a substrate bias of -150 V.

Figure 5 shows the cross-sectional and surface morphologies of the Ti-N thin films deposited on Si at floating and a substrate bias of -150 V. These Ti-N thin films had a compact structure without any defects such as holes or cracks. The surfaces of the Ti-N thin films deposited at floating and a substrate bias of -150 V were smooth, without any defects, such as particles or cracks, appearing on them. A columnar structure can be observed in the cross-sectional images of the Ti-N thin films, and the column size of the thin film deposited at a substrate bias of -150 V is smaller than that deposited at floating. It should be noted that the thin film deposited at a substrate bias of -150 V is denser than that deposited at floating. By applying a substrate bias of -150 V, the strong ion bombardment not only decreased the column size of the Ti-N thin film, but also densified the thin film.

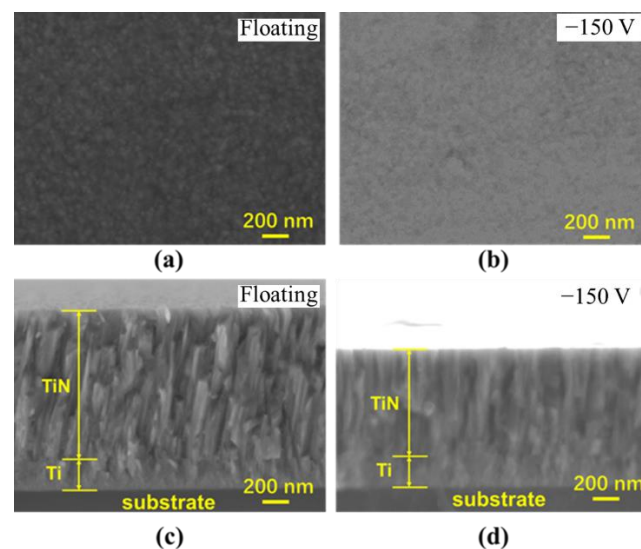


Figure 5. Surface (a,b) and cross section (c,d) scanning electron microscopy images of the TiN thin films deposited at floating and a substrate bias of -150 V.

Figure 6 shows the AFM morphologies of the Ti-N thin films deposited on Si at floating and a substrate bias of -150 V. The root mean square (RMS) surface roughness of these thin films was less than 2.5 nm. The surface roughness of the Ti-N thin films deposited at a substrate bias of -150 V was lower than that deposited at floating, which can be attributed to the bombardment of the thin film surface by high-energy ions, which resulted in a smoother surface.

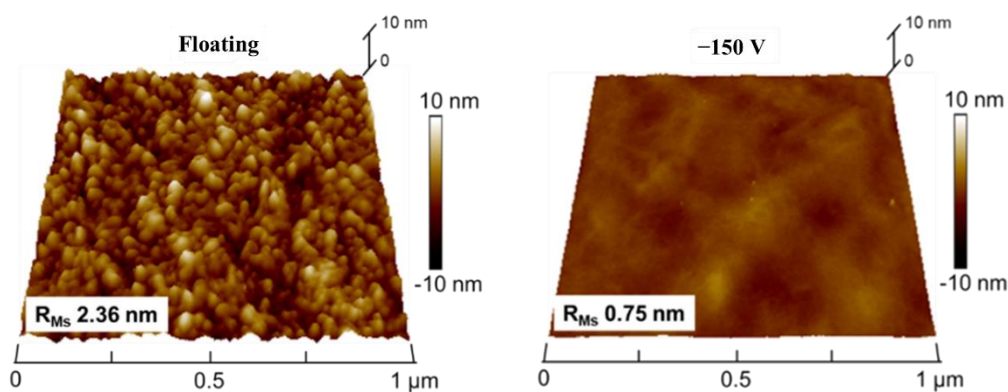


Figure 6. Atomic force microscopy images of the TiN thin films deposited at floating and a substrate bias of -150 V.

Figure 7 shows the deposition rate and residual stress of the Ti-N thin films deposited on Si at floating and a substrate bias of -150 V. The deposition rate of the Ti-N thin film deposited at floating was 33.5 nm/min whereas the deposition rate decreased to 31.5 nm/min when the substrate bias applied was -150 V. During the film deposition, when the ion energy was increased by applying higher substrate bias, the energized ions re-sputtered and etched the growth film, which reduced the thin film deposition rate.

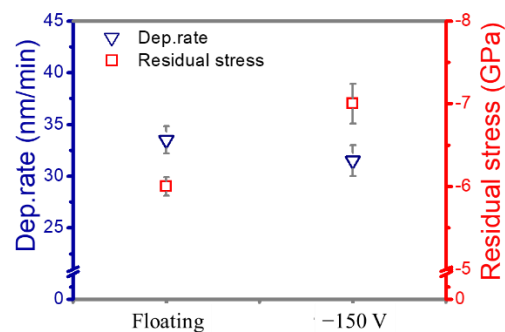


Figure 7. Deposition rate and residual stress of the TiN thin films deposited at floating and a substrate bias of -150 V.

All Ti-N thin films were under compressive stress, which was consistent with the shift of the (111) diffraction peak in the XRD results. The compressive stress was -6 GPa when the Ti-N thin film was deposited at floating and was -7 GPa at a substrate bias of -150 V. The bombardment and implantation effect of the high-energy ions generate compressive residual stress in the Ti-N thin films; the higher the ion energy, the more noticeable the effect of the bombardment and implantation, and the larger the compressive residual stress. Therefore, applying a substrate bias of -150 V generated more compressive residual stress in the Ti-N thin film than at floating.

Figure 8 shows the scratch topographies of the Ti-N thin films deposited on SS at floating and a substrate bias of -150 V. For the Ti-N thin film deposited at floating, the peel-off of the Ti-N thin film occurred at the scratch at a load of 70 N and at a bias of -150 V, the peel-off occurred at a load of 20 N. These results indicate that the adhesion strength of the Ti-N thin film deposited at floating is better than that deposited at a substrate bias of -150 V. For brittle ceramic thin films, the compressive residual stress can decrease the adhesion strength between the thin film and the substrate. In this study, the compressive residual stress of the Ti-N thin film deposited at a substrate bias of -150 V was higher than that at floating. Thus, the Ti-N thin film deposited at a substrate bias of -150 V is more likely to suffer catastrophic failure, such as peel-off, during a scratch test.

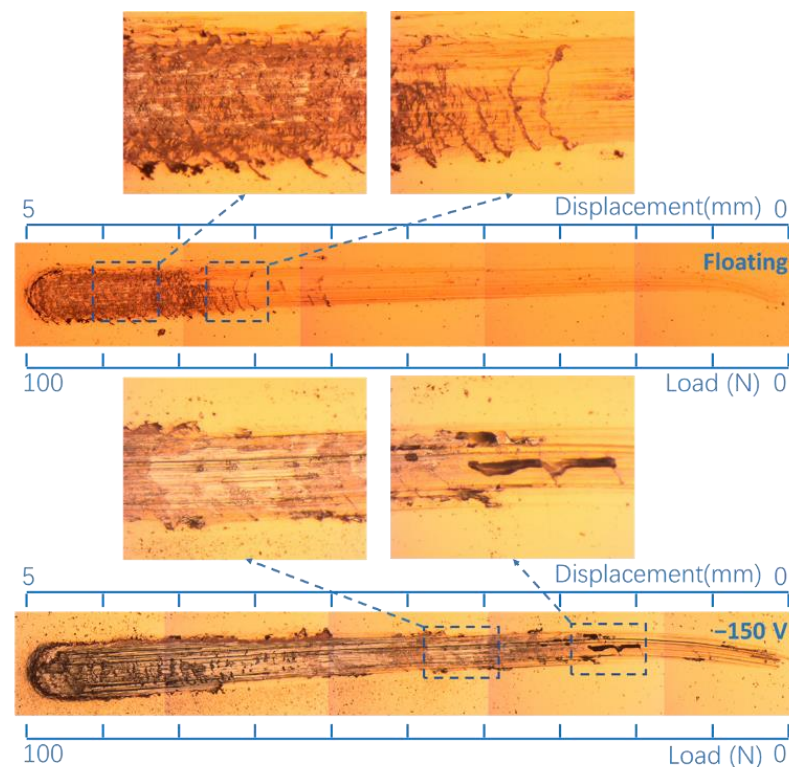


Figure 8. Scratch topographies of the TiN thin films deposited at floating and a substrate bias of -150 V.

4. Conclusions

In this study, Ti-N thin films were deposited using HPPMS. The target discharge and plasma characteristics before and after the introduction of nitrogen gas were analyzed. The effect of the ion energy on the microstructure, residual stress, and adhesion of the thin films was studied. The results demonstrate that with the introduction of nitrogen gas, the Ti target discharge current and peak power increased, the total flux of the Ti species decreased, and the ionized ratio of Ti increased. The Ti-N thin film deposited by HPPMS was dense and defect-free. When the energy of the Ti ions was increased, the grain size and surface roughness of the Ti-N film decreased, the residual stress increased, and the adhesion strength of the Ti-N thin film decreased.

Author Contributions: Conceptualization, Y.L.; methodology, D.M.; investigation, D.M. and Q.D.; writing—original draft preparation, D.M. and H.L.; writing—review and editing, Y.L.; supervision, Y.L.; funding acquisition, D.M. and Y.L. All authors have read and agreed to the published version of the manuscript.

Funding: This work was supported by NSFC (52072312), Sichuan Science and Technology Project (2020YFH0044) and (2021YFH0032), and Science and Technology on Surface Physics and Chemistry Laboratory (No.6142A02190402).

Institutional Review Board Statement: Not applicable.

Informed Consent Statement: Not applicable.

Data Availability Statement: Available on request from corresponding author.

Conflicts of Interest: The authors declare no conflict of interest.

References

1. Veprek, S.; Veprek-Heijman, M.G.J.; Karvankova, P.; Prochazka, J. Different approaches to superhard coatings and nanocomposites. *Thin Solid Films* **2005**, *476*, 1–29. [[CrossRef](#)]
2. Ghailane, A.; Makha, M.; Larhlimi, H.; Alami, J. Design of hard coatings deposited by HiPIMS and dcMS. *Mater. Lett.* **2020**, *280*, 5. [[CrossRef](#)]
3. Ghailane, A.; Larhlimi, H.; Tamraoui, Y.; Makha, M.; Busch, H.; Fischer, C.B.; Alami, J. The effect of magnetic field configuration on structural and mechanical properties of TiN coatings deposited by HiPIMS and dcMS. *Surf. Coat. Technol.* **2020**, *404*, 10. [[CrossRef](#)]
4. Hovsepian, P.E.; Sugumaran, A.A.; Purandare, Y.; Loch, D.A.L.; Ehiasarian, A.P. Effect of the degree of high power impulse magnetron sputtering utilisation on the structure and properties of TiN films. *Thin Solid Films* **2014**, *562*, 132–139. [[CrossRef](#)]
5. Gudmundsson, J.T.; Brenning, N.; Lundin, D.; Helmersson, U. High power impulse magnetron sputtering discharge. *J. Vac. Sci. Technol. A* **2012**, *30*, 030801. [[CrossRef](#)]
6. Sarakinos, K.; Alami, J.; Konstantinidis, S. High power pulsed magnetron sputtering: A review on scientific and engineering state of the art. *Surf. Coat. Technol.* **2010**, *204*, 1661–1684. [[CrossRef](#)]
7. Lundin, D.; Sarakinos, K. An introduction to thin film processing using high-power impulse magnetron sputtering. *J. Mater. Res.* **2012**, *27*, 780–792. [[CrossRef](#)]
8. Elmkhah, H.; Attarzadeh, F.; Fattah-Alhosseini, A.; Kim, K.H. Microstructural and electrochemical comparison between TiN coatings deposited through HIPIMS and DCMS techniques. *J. Alloys Compd.* **2018**, *735*, 422–429. [[CrossRef](#)]
9. Ding, J.; Yin, X.; Fang, L.; Meng, X.; Yin, A. TiN Films Deposited on Uranium by High Power Pulsed Magnetron Sputtering under Low Temperature. *Materials* **2018**, *11*, 1400. [[CrossRef](#)]
10. Wu, J.; Wu, B.H.; Ma, D.L.; Xie, D.; Wu, Y.P.; Chen, C.Z.; Li, Y.T.; Sun, H.; Huang, N.; Leng, Y.X. Effects of magnetic field strength and deposition pressure on the properties of TiN films produced by high power pulsed magnetron sputtering (HPPMS). *Surf. Coat. Technol.* **2017**, *315*, 258–267. [[CrossRef](#)]
11. Diyatmika, W.; Liang, F.-K.; Lou, B.-S.; Lu, J.-H.; Sun, D.-E.; Lee, J.-W. Superimposed high power impulse and middle frequency magnetron sputtering: Role of pulse duration and average power of middle frequency. *Surf. Coat. Technol.* **2018**, *352*, 680–689. [[CrossRef](#)]
12. Ghasemi, S.; Farhadzadeh, A.R.; Ghomi, H. Effect of frequency and pulse-on time of high power impulse magnetron sputtering on deposition rate and morphology of titanium nitride using response surface methodology. *Trans. Nonferrous Met. Soc. China* **2019**, *29*, 2577–2590. [[CrossRef](#)]
13. Greczynski, G.; Jensen, J.; Böhlmark, J.; Hultman, L. Microstructure control of CrN_x films during high power impulse magnetron sputtering. *Surf. Coat. Technol.* **2010**, *205*, 118–130. [[CrossRef](#)]
14. Tillmann, W.; Grisales, D.; Stangier, D.; Thomann, C.A.; Debus, J.; Nienhaus, A.; Apel, D. Residual stresses and tribomechanical behaviour of TiAlN and TiAlCN monolayer and multilayer coatings by DCMS and HiPIMS. *Surf. Coat. Technol.* **2021**, *406*, 12. [[CrossRef](#)]
15. Zhang, Y.K.; Feng, A.X.; Lu, J.Z.; Kong, D.J.; Tang, C.P. Nondestructive measurement of the residual stress TiN thin film coated on AISI 304 substrate by X ray stress analyzer. In *Ico20: Materials and Nanostructures*; Lu, W., Young, J., Eds.; Proceedings of SPIE; Spie-Int Soc Optical Engineering: Bellingham, DC, USA, 2006; Volume 6029.
16. Jing, F.J.; Yin, T.L.; Yukimura, K.; Sun, H.; Leng, Y.X.; Huang, N. Titanium film deposition by high-power impulse magnetron sputtering: Influence of pulse duration. *VACUUM* **2012**, *86*, 2114–2119. [[CrossRef](#)]
17. Ma, D.L.; Li, Y.T.; Deng, Q.Y.; Huang, B.; Leng, Y.X.; Huang, N. Tailoring the texture of titanium thin films deposited by high-power pulsed magnetron sputtering. *Int. J. Mod. Phys. B* **2019**, *33*, 1940017. [[CrossRef](#)]
18. Jiang, F.; Chen, S.; Leng, Y.; Huang, N. Effect of wafer size on the film internal stress measurement by wafer curvature method. *J. Wuhan Univ. Technol. Mater. Sci. Ed.* **2016**, *31*, 93–99. [[CrossRef](#)]
19. Musil, J. Role of energy in low-temperature high-rate formation of hydrophilic TiO₂ thin films using pulsed magnetron sputtering. *J. Vac. Sci. Technol. A* **2007**, *25*, 666–674. [[CrossRef](#)]
20. Moreira, M.A.; Törndahl, T.; Katardjiev, I.; Kubart, T. Deposition of highly textured AlN thin films by reactive high power impulse magnetron sputtering. *J. Vac. Sci. Technol. A Vac. Surf. Film.* **2015**, *33*, 021518. [[CrossRef](#)]
21. Saringer, C.; Franz, R.; Zorn, K.; Mitterer, C. Effect of discharge power on target poisoning and coating properties in reactive magnetron sputter deposition of TiN. *J. Vac. Sci. Technol. A* **2016**, *34*, 8. [[CrossRef](#)]
22. Magnus, F.; Sveinsson, O.B.; Olafsson, S.; Gudmundsson, J.T. Current-voltage-time characteristics of the reactive Ar/N₂ high power impulse magnetron sputtering discharge. *J. Appl. Phys.* **2011**, *110*, 083306. [[CrossRef](#)]
23. Ma, D.L.; Liu, H.Y.; Deng, Q.Y.; Yang, W.M.; Silins, K.; Huang, N.; Leng, Y.X. Optimal target sputtering mode for aluminum nitride thin film deposition by high power pulsed magnetron sputtering. *Vacuum* **2019**, *160*, 410–417. [[CrossRef](#)]
24. Čada, M.; Lundin, D.; Hubička, Z. Measurement and modeling of plasma parameters in reactive high-power impulse magnetron sputtering of Ti in Ar/O₂ mixtures. *J. Appl. Phys.* **2017**, *121*, 171913. [[CrossRef](#)]
25. Zheng, B.C.; Wu, Z.L.; Wu, B.; Li, Y.G.; Lei, M.K. A global plasma model for reactive deposition of compound films by modulated pulsed power magnetron sputtering discharges. *J. Appl. Phys.* **2017**, *121*, 171901. [[CrossRef](#)]

26. Jiang, F.; Zhang, T.F.; Wu, B.H.; Yu, Y.; Wu, Y.P.; Zhu, S.F.; Jing, F.J.; Huang, N.; Leng, Y.X. Structure, mechanical and corrosion properties of TiN films deposited on stainless steel substrates with different inclination angles by DCMS and HPPMS. *Surf. Coat. Technol.* **2016**, *292*, 54–62. [[CrossRef](#)]
27. Chawla, V.; Jayaganthan, R.; Chandra, R. Structural characterizations of magnetron sputtered nanocrystalline TiN thin films. *Mater. Charact.* **2008**, *59*, 1015–1020. [[CrossRef](#)]
28. Rauschenbach, B.; Gerlach, J.W. Texture development in titanium nitride films grown by low-energy ion assisted deposition. *Cryst. Res. Technol.* **2000**, *35*, 675–688. [[CrossRef](#)]
29. Zhitomirsky, V.N.; Grimberg, I.; Rapoport, L.; Boxman, R.L.; Travitzky, N.A.; Goldsmith, S.; Weiss, B.Z. Bias voltage and incidence angle effects on the structure and properties of vacuum arc deposited TiN coatings. *Surf. Coat. Technol.* **2000**, *133–134*, 114–120. [[CrossRef](#)]
30. Mahieu, S.; Depla, D. Reactive sputter deposition of TiN layers: Modelling the growth by characterization of particle fluxes towards the substrate. *J. Phys. D Appl. Phys.* **2009**, *42*, 053002. [[CrossRef](#)]